Published in final edited form as:
J Magn Reson Imaging. 2011 August ; 34(2): 262–269. doi:10.1002/jmri.22624.

Implementation of Multi-Echo Based Correlated Spectroscopic Imaging and Pilot Findings in Human Brain and Calf Muscle

Gaurav Verma, MS[1], **Scott Lipnick, PhD**[2], **Saadallah Ramadan, PhD**[3], **Rajakumar Nagarajan, PhD**[2], and **M. Albert Thomas, PhD**[1,2]

[1]Department of Bioengineering, University of California, Los Angeles, CA 90095, USA

[2]Department of Radiological Sciences, University of California, Los Angeles, CA 90095, USA

[3]Department of Radiology, Brigham & Women Hospital, Boston, MA, 02115, USA

Abstract

Purpose—To implement a spatially-encoded Correlated Spectroscopic Imaging (COSI) sequence on 3T MRI/MRS scanners incorporating four echoes to collect four phase-encoded acquisitions per repetition time (TR), and to evaluate the performance and reliability of this four-dimensional (4D) Multi-Echo COSI (ME-COSI) sequence in brain and calf muscle.

Materials and Methods—Typical scan parameters for the 4D datasets were as follows: TR=1500ms, 2000 Hz bandwidth, 8×8 spatial encoding, one average, 64 Δt_1 increments and the scan duration was 25 minutes. The performance and test-retest reliability of ME-COSI were evaluated with phantoms and in the occipito-parietal brain tissues and calf of six healthy volunteers (mean age = 32 years old).

Results—Regional differences in concentrations of lipids, creatine (Cr), choline (Ch) and carnosine (Car) were observed between spectra from voxels located in tibial marrow, tibialis anterior and soleus muscle. Diagonal and cross peak resonances were identified from several brain metabolites including N-acetyl aspartate (NAA), Ch, Cr, lactate (Lac), aspartate (Asp), glutathione (GSH) and glutamine\glutamate (Glx). Coefficients of variation (CV) in metabolite ratios across repeated measurements were <15% for diagonal and <25% for cross-peaks observed *in vivo*.

Conclusion—The ME-COSI sequence reliably acquired spatially-resolved two-dimensional (2D) Correlated Spectroscopy (COSY) spectra demonstrating the feasibility of differentiating spatial variation of metabolites in different tissues. Multi-echo acquisition shortens scan duration to clinically feasible times.

Keywords

Multi Spin Echo; 2D Correlated Spectroscopy; Spectroscopic Imaging; Brain; Calf muscle

INTRODUCTION

Two-dimensional (2D) magnetic resonance spectroscopy (MRS) (1–2) has facilitated improved detection of metabolites compared to one-dimensional (1D) MRS by taking advantage of J-coupling interactions between protons of metabolites and resolving co-

Address for Correspondence: M. Albert Thomas Ph.D., Radiological Sciences, David Geffen School of Medicine at UCLA, 10833 Le Conte Avenue, Los Angeles, CA 90095-1721, Tel: (310) 206 4191, Fax: (310) 825 5837, athomas@mednet.ucla.edu.

#Presented at the 50th ENC Meeting, Asilomar, California, March 29-April 3, 2009 and the 17th ISMRM Meeting, Honolulu, Hawaii, April 18–24, 2009

resonant metabolites due to the added 2nd spectral dimension. 2D MRS *in vivo* studies using localized correlated spectroscopy (L-COSY) have shown spectral separation in many clinically-relevant metabolites often obscured in 1D MRS including lactate (Lac), glutathione (GSH), glutamate/glutamine (Glx) and myo-inositol (mI) (3–5) in brain and intra- and extra-myocellular lipids (IMCL and EMCL) in calf muscle (6–7). When combined with multi-voxel spatial encoding, the resulting magnetic resonance spectroscopic imaging (MRSI) (8–10) sequence has the potential to provide spatial information about a range of metabolites difficult to resolve with 1D MRS.

2D MRS adds a second spectral dimension by incorporating an incremented time delay to indirectly monitor the t_1 evolution (1,11). Coherence may develop between coupled spins during the t_1 evolution and transfer from one coupled spin to another before being measured during t_2 evolution. Multiple Δt_1 increments, typically 50 to 100 depending on the desired resolution, are acquired with incremented delays and a Fourier transform is applied along these time points to generate the 2nd (F_1) spectral dimension. With a repetition time (TR) of 1500 ms, the total duration for the single-voxel based L-COSY is 15–26 minutes (3–5), depending on the desired resolution. Using phase-encoding gradients to spatially encode the L-COSY sequence, 2D COSY spectra can be recorded in multiple locations, a process that would take an hour or more using the conventional L-COSY approach. Multi-Echo (ME) encoding schemes, like turbo spin echo (TSE) and fast spin echo (FSE) (12–14), have demonstrated dramatic reductions in overall scan time in magnetic resonance imaging (MRI). Similar approaches in 1D MRSI have demonstrated the applicability of ME techniques to spectroscopy (15–16). One limiting factor for ME spectroscopy is the T_2 decay as the signal is greatly diminished with each echo, especially in living tissues where T_2 relaxation times are shorter (17–18).

The purpose of this study was to develop a novel four-dimensional (4D) MRSI sequence combining two spectral dimensions with two spatial dimensions and incorporating ME for encoding one of the spatial dimensions to reduce scan times to suit clinical requirements. This sequence was first tested for sensitivity and reproducibility *in vitro* using physiological phantoms. Pilot feasibility of recording multi-voxel based 2D COSY was tested *in vivo* in the calf and brain of healthy volunteers.

MATERIALS AND METHODS

The multi-voxel 4D MRSI pulse sequence that was developed incorporates four echoes per repetition to accelerate the overall acquisition rate. Figure 1 shows the pulse sequence diagram, hereafter referred to as Multi-Echo Correlated Spectroscopic Imaging (ME-COSI). At the core of ME-COSI is the L-COSY module containing three slice-selective radio frequency (RF) pulses (90°–180°-Δt_1-90°) with a time delay to indirectly encode the t_1 dimension before the last coherence transfer 90° RF pulse (3–5). This time delay is incremented by a fixed value (Δt_1) such that the effective echo time (TE) of each repetition progressively increases over all the t_1 increments.

Three 180° RF pulses are applied after the first acquisition resulting in a total echo train length (ETL) of four including the coherence transfer echo (CTE) after the volume localizing three RF pulses. Phase encoding gradients are applied as follows: *a) 1st spatial dimension*: first after the slice-selective 90° RF pulse and 2nd through 4th before and after each refocusing pulse, allowing the encoding of four k-space locations per TR. The whole cycle is repeated again to acquire a full row in k-space, encompassing eight encoding steps, in two repetitions. Because T_2 attenuation diminishes the signal intensity of echoes later in each repetition (19–20), the central areas of k-space, where more signal is expected, are acquired earlier in each TR and outer areas are acquired later as previously described by

Duyn et al. (15) *b) 2nd spatial dimension*: eight repetitive encoding steps after the slice-selective 90° RF pulse. Multi-echo encoding was confined to one spatial dimension for ease of processing and to limit the spatial distortion caused by the T_2 weighting to that dimension.

Typical scan parameters for the ME-COSI sequence are: TE = 30ms, TR = 1500ms, F_2 bandwidth = 2000 Hz, complex points = 256, spatial array size = 8×8 and 50 to 100 Δt_1 increments of 0.8ms with one average per increment resulting in an F_1 bandwidth of 1250 Hz. *In vivo* studies featured fields-of-view (FOV) of 80mm in the anterior-posterior and left-right dimensions with slice thickness of 40mm for the brain and 20mm for the calf in thickness, yielding voxel sizes of 4.0 ml in the brain and 2.0 ml in the calf. *In vitro* scan voxels were typically 0.98 to 2.0 ml in volume. Total scan times were 20 min. in the calf, 25 min. in the brain and 40 min. in phantoms, reflecting the 50, 64 and 100 Δt_1 increments acquired in each type of scan, respectively.

The 90° excitation pulse was 2.6 ms long and had an excitation bandwidth of 3365 Hz, while the 180° refocusing pulse was 4.4 ms long and had an excitation bandwidth of 1363 Hz. The center frequency for the ME-COSI scans was placed at 2.7 ppm to minimize chemical shift displacement.

All scans were performed on a 3T Tim-Trio (Siemens Medical Solutions, Erlangen, Germany) whole-body scanner running on the VB15A platform. Global water suppression was achieved by the water suppression enhanced through T_1 effects (WET) (21) technique and outer volume suppression (OVS) was used to suppress undesired signal from areas like skull marrow (22). The sequence was initially tested for compatibility with a number of coils including a single-channel circularly polarized (CP) extremity coil, an 8-channel “receive” knee array, and 8-channel & 12-channel “receive” head coils. The 8-channel head coil was empirically observed to be the most sensitive coil, and was large enough to facilitate *in vivo* scans of the whole brain and was thus selected to perform reproducibility studies with the brain phantom.

Phantom Studies

Phantom studies of the ME-COSI sequence were categorized into two types: testing for spectral sensitivity and testing for spatial specificity. Spectral sensitivity tests were conducted by scanning a gray matter brain phantom containing sixteen metabolites at physiological concentrations (23), hereafter referred to as the ‘brain phantom’. To test the sequence for reproducibility, thirty-two scans of the brain phantom were performed with the 8-channel head coil over five non-consecutive days. The scans consisted of an 8×8 spatial array with 256 complex points and 100 Δt_1 increments, and each scan lasted 40 minutes. The FOV was 80mm × 80mm with a slice thickness of 20mm, yielding a voxel size of 2.0 ml. T_1-weighted and spin-echo- based magnetic resonance imaging (MRI) scans with a total scan time of two minutes were used to localize the voxels. For each scan, the phantom was positioned at the center of the magnet, and the voxel array was likewise placed at the isocenter.

Testing for spatial specificity was performed by scanning an inhomogeneous phantom consisting of four containers with metabolite solutions – N-acetyl aspartate (NAA), creatine (Cr), choline (Ch) and lactate (Lac) – arranged in a square configuration and submerged inside a water bath, hereafter referred to as the ‘quad phantom’. Five scans were performed on the quad phantom, with a typical FOV of 112mm × 112mm and a thickness of 5mm, resulting in a 0.98ml voxel size. The positions of the component phantoms were varied in different scans to confirm that reconstructed spectra matched these configurations.

Human Volunteer Studies

Two regions were selected for testing the ME-COSI sequence: the brain and the calf. For each region, *in vivo* trials were performed on six healthy volunteers (mean age = 32 years). Similar to the phantom scans, voxel localization was accomplished with T_1-weighted spin-echo MRI scans. Using these images, an 8×8 spatial array was placed in the desired region. For brain studies, the array was localized in the occipital lobe, immediately posterior to the ventricles, while avoiding inclusion of the skull marrow. To investigate the test-retest reliability of the ME-COSI sequence in human brain, five scans of one volunteer were performed to represent an intra-subject study. An inter-subject study was also conducted involving four healthy volunteers who were scanned with the ME-COSI sequence in the same location and with the same parameters.

For calf studies, a transverse cross-section was obtained at the area of greatest extent of muscle tissue. In particular, the tibia, fibula and soleus and gastrocnemius muscles were identified and placed within the volume of interest (VOI). For brain and calf studies, manual B_0 shimming was performed to improve the field homogeneity, and spatial saturation bands were applied where necessary to reduce signal contamination from skull marrow or excess subcutaneous lipids in the calf.

Data Analysis

Raw data obtained from the scanner was post-processed using a custom MATLAB-based (The Mathworks, Natick, MA, USA) signal processing package. Figure 2 shows the post-processing steps involved in reconstructing the raw data into measurable spectra. Raw data retrieved from the scanner were processed in MATLAB through a series of steps including scaling by a constant value, spatial reordering, resolving averages and oversampling (24), phase correction, coil combination and Eddy current correction (25). A spatial Hamming filter was applied to the data in k-space and Fast Fourier Transforms (FFTs) were applied across the dimensions k_x and k_y to yield the spatial dimensions x (left to right) and y (anterior to posterior), respectively. No zero-filling was applied on either spatial dimension and the final dataset reflected the acquired 8×8 resolution. Zero-filling by a factor of two was applied along both spectral dimensions followed by skewed sine-bell exponential filters (skew = 0.5) for line-broadening. A Fourier transform was then applied twice, along the time dimensions t_1 and t_2 to yield the spectral dimensions F_1 and F_2, respectively.

The final spectra comprised a 4D matrix arranged in the format $S(F_2, x, y, F_1)$. These spectra were plotted and analyzed in both MATLAB and the NMR-specific plotting program Felix (Felix NMR, San Diego, CA, USA). Quantitative measurements were obtained by calculating volume integrals for peaks identified in the 2D spectra. The same peak positioning table was used across all scans to ensure objective peak selection.

RESULTS

Figure 3 shows the spatial distribution of the diagonal peaks due to choline (Ch, F_1=F_2=3.2 ppm), creatine (Cr, F_1=F_2=3.0 ppm), and N-acetyl aspartate (NAA, F_1=F_2=2.0 ppm) and the cross peak of lactate (Lac, F_1=1.3, F_2=4.1 ppm) against their physical location within the quad phantom. In all figures showing voxel localization, the yellow arrow indicates the ME-encoded dimension. Over five separate scans of the quad phantom, the reconstructed spatial profiles closely resembled the geometric configuration of the component metabolites. Evidence of spatial blurring in the ME-encoded direction was evident in some of the metabolite profiles extracted from both phantoms and *in vivo* data. The extent of this blurring was dependent on the contour levels selected for the data plots and more blurring was observed in the profile of Ch than for the other metabolites in the quad phantom. As

shown in Figure 3, this occaisonally caused some signal to appear outside the excitation volume. Some evidence of voxel misregisteration due to chemical shift (26) was also visible as some metabolite profiles appeared displaced from the physical location of the phantom.

Figure 4 shows extracted ME-COSI spectra from the tibial bone marrow and the soleus muscle. Tables 1 and 2 contain various chemical shifts of 2D diagonal and cross peaks (7) form bone marrow and calf muscle, respectively. The bone marrow peaks are designated C' and D' for cross peaks and diagonal peaks respectively, whereas the muscle peaks are designated C and D. The marrow spectrum was characterized by dominant lipid peaks including the poly-methylene protons of fat centered at 1.3 ppm, the triglyceride backbone at 4.2 ppm, olefenic protons at 5.4 ppm and their cross peaks at (F_1,F_2 = 2.2, 5.4 ppm) (C1') and (F_1,F_2 = 2.9, 5.4 ppm) (C2'). By contrast, muscle spectra showed the presence of Cr at 3.0 ppm (D8) and 3.9 ppm (D11), Ch at 3.2 ppm (D9) and carnosine (Car) at 8.0 ppm (D16), none of which were detected in the tibial bone marrow. Lipid peaks were visible though less dominant than those in the marrow, with extra-myocellular lipids (EMCL) (C3 and C4) and also IMCL (C1 and C2) cross-peaks, not visible in the marrow. Some residual water signal was visible in the muscle spectra despite WET-based water suppression, but no water signal was detected in the bone marrow. Spectra from the fibula showed a similar composition to the larger tibia, but were subject to partial volume effects due to the presence of some muscle within the 2.0 ml voxel.

Figure 5 shows the spatial distribution of the 3.9 ppm diagonal peak due to N-methylene protons of Cr across the 8×8 data set. The spatial profiles of the Cr resonance showed the residual dipole-dipole splitting effect in the region of the tibialis anterior muscle as shown by Kreis et al. (27). Cr was detected all throughout the VOI, except in the area of the tibial marrow.

Figure 6 shows a typical ME-COSI spectrum obtained from a central voxel in the occipital lobe of a 27 year-old healthy male volunteer. Diagonal peaks due to Lac, NAA, Ch, Cr and residual water, as well as cross-peaks due to aspartate (Asp), γ-aminobutyric acid and macromolecules (GABA/MM), glutamate/glutamine (Glx), lactate/threonine (Lac/Thr), myo-inositol (mI), myo-Inositol-choline (mICh), NAA and phosphoethanolamine (PE) have all been labeled. Metabolite peaks were visible throughout the volume of excitation, but showed noted hypointensity in the voxels containing ventricular cerebrospinal fluid (CSF), where residual water was the dominant signal.

Figure 7 shows the spatial distribution of the 3.0 ppm diagonal peak of Cr and the cross peaks of Glx at [F_1, F_2] = 2.0, 3.6 ppm and mI at [F_1, F_2] = 3.0, 3.5 ppm. in the profiles were extracted from ME-COSI data taken in the occipital lobe of a healthy 24-year old and superimposed against a T1-weighted MRI. Hypointensity in the peaks of Glx and other metabolites was observed in voxels containing cerebrospinal fluid (CSF), for example in the area of the ventricles.

Table 3 shows the coefficients of variation (CVs) in the ratio of signal from various metabolites to the signal from the 3.0 ppm diagonal peak of creatine (S/S_{Cr}). These CVs were recorded across 32 scans of the brain phantom using 2.0ml voxels. A single central voxel was studied to test the reproducibility of data across numerous scans, and the same data analysis was performed in a neighboring central voxel from the brain phantom with similar results.

The CVs of the major diagonal peaks from the brain phantom ranged from 5–12%. Of these, the 2.0 ppm diagonal peak due to NAA showed the lowest CV at 5% and the 1.3 ppm diagonal peak of Lac the highest at 12%. When cross-peaks above and below the diagonal were consistently visible above the background noise, their signals were averaged into a

combined value. Combined cross peaks showed CVs ranging from 5.3% for Glx to 12% for GABA/MM. Water suppression centered at $[F_1,F_2]$ = 4.7 ppm affected the above-the-diagonal cross-peaks of GSH at $[F_1, F_2]$ = 4.5, 2.9 ppm and Lac at $[F_1, F_2]$ = 4.1, 1.3 ppm, precluding their measurement. Thus, only cross-peaks below the diagonal were measured for these metabolites. The peaks due to GSH had a CV of 17% and those from Lac had a CV of 25%.

Table 4 shows the CVs of S/S_{Cr} across *in vivo* studies of human brain. In the intra-subject study, in which the occipital lobe of one volunteer was scanned five times, the CVs of the measured metabolites ranged from 4–7% for major diagonal peaks and 9–17% for cross peaks. CVs for Lac and GSH were not measured for this study because their peaks were often obscured by the more dominant nearby peaks of lipids at 1.3 ppm and water at 4.7 ppm, respectively. CVs from the inter-subject study, where four volunteers were scanned with the ME-COSI sequence, were on average 31% higher than their intra-subject counterparts. CVs for the S/S_{Cr} of the diagonal peaks of Cr, mI, Ch and NAA ranged from 6–9%. CVs for the cross peaks of NAA, Glx, PE, Asp and GABA/MM ranged from 12–18%.

DISCUSSION

In vitro studies using the quad phantom showed well-separated spatial profiles from each of the four metabolites comprising the quad phantom. Studies in both the brain phantom and occipital lobe were able to reliably identify a large number of metabolite resonances (5,28), including cross-peaks due to *J*-coupling not observable with 1D MRS. Several of these cross-peaks identifiable in 2D MRS, like PE and Lac, have been demonstrated to be clinically relevant, including oncological studies of the brain (29–30).

Reproducibility studies both in phantoms with 2.0 ml voxels and in human brain at 4.0 ml showed CVs of most diagonal peaks to be under 15% and most cross peak CVs to be under 25%. More minute differences in concentration could be measured by improving signal-to-noise ratio (SNR) either with multiple averages or a larger voxel size. Although ME-COSI data may be subject to baseline distortions, these affect 2D MRS data differently than 1D data. The second spectral dimension in ME-COSI allows a greater degree of spectral separation from the peaks of water and metabolites. This minimizes the effect of even poorly-suppressed water on the integral volume measurements of other peaks.

Peaks due to Car, Ch, Cr, IMCL and EMCL were visible in voxels localized within muscle, but not those localized within bone marrow. In contrast, lipid peaks (methyl, methylene, triglycerides, olefenic protons etc.) appeared significantly more dominant in the marrow as compared to the muscle. Peak splitting due to residual dipole-dipole interaction was observed in the 3.0 and 3.9 ppm peaks of Cr in the region of the tibialis anterior, consistent with previous 2D MRS studies (27, 31).

In addition to the diagonal peaks of Cr, Ch, NAA, Lac and mI, several cross peaks were detectable in the brain with ME-COSI, including those due to NAA, Glx, mI, PE, Asp, Lac and GABA and macromolecules. The spatial distribution of these peaks generally showed signal throughout the excitation volume with hypointensity in the voxels near the ventricles. The relatively coarse spatial resolution of the ME-COSI sequence precluded isolating voxels entirely within the ventricles, and the resulting data shows partial volume effects with both CSF and cerebral tissue contributing to signal in the area of the ventricles.

Because acquisitions from the outer parts of k-space were acquired later in each TR, there is an intrinsic T_2 weighting in the data especially noticeable where T_2 relaxation times are shorter. The outer portions of k-space therefore experience heavier T_2 attenuation, resulting

in blurring along the multi-echo encoded direction after an FFT is applied (32), especially in metabolites with shorter T_2 constants like Ch. This blurring effect can be further complicated by the displacement artifacts common to chemical shift imaging sequences.

With a 128 ms (2000 Hz bandwidth, 256 complex points) long readout window and an echo spacing of 138 ms, the final echo is acquired approximately 440 ms after the initial excitation. Applying T_2 decay constants of 156 ms for Ch, 187 ms for Cr and 295 ms for NAA at 3T (33) along with the timing of the ME-COSI sequence, the theoritical signal loss due to T_2 decay can be calculated for each echo. NAA loses 10%, 43%, 65% and 78% of its undecayed signal strength across the four echoes. Cr loses 15%, 59% 80% and 91% and Ch loses 17%, 66%, 86% and 94% of their signal strength across the four echoes. Restricting the later echoes to the outer parts of k-space mitigates the loss of signal by ensuring the central parts of k-space, where more signal is expected, are the least affected by T_2 attenuation. 2D spectroscopy incorporates Δt_1 delays, effectively increasing the TE of later measurements and further contributing to this signal loss.

The effects of T_2 attenuation were also tested experimentally with a conventional CSI sequence and a 1D analogue of ME-COSI with only one increment and with the last localized pulse changed to 180°. The two sequences were applied in a scan of the brain phantom with otherwise identical parameters. The ratio of signal intensity of NAA, Ch and Cr between ME-COSI and CSI were found to be 73.4%, 71.3% and 71.9%, respectively in the central voxels and all metabolite profiles showed blurring along the multi-echo encoded dimension. The NAA/Cr and Ch/Cr ratios were 1.935 and 0.770 for CSI and 1.991 and 0.765 for ME-COSI.

Line-widths in the real and imaginary components of the ME-COSI data ranged from 10 to 15 Hz *in vivo* and 3 to 7 Hz in phantoms. As a consequence of unavoidable artifacts like thermal noise and motion, spectral quality was somewhat poorer in the human compared to phantom studies, having wider metabolite peaks, T_1 ridging around the dominant singlet peak of unsuppressed water and occasional lipid contamination from skull marrow or subcutaneous fat.

ME-COSI demonstrated reproducibility comparable to the single-voxel L-COSY sequence, but improves on L-COSY by detecting from multiple locations. The recently introduced echo-planar COSI (EP-COSI) (34) sequence has demonstrated faster acquisition and higher resolution than ME-COSI. Echo planar encoding, however, is reliant on rapid gradient switching, which leaves the sequence more susceptible to eddy currents (35) and limits the F_2 bandwidth based on the slew rate. This can be especially problematic at higher field strengths, where increased spectral separation demands proportionally increased bandwidths.

Further improvements in the sequence are possible through application of existing acceleration techniques to ME-COSI. Parallel acquisition schemes, like sensitivity encoding (SENSE), have been incorporated in 1D MRSI to substantially accelerate signal acquisition in phased array coils (36). A critical limitation of ME-COSI is the readout time associated with MR spectroscopy. At 3T, a typical readout takes 128ms to acquire 256 complex points to cover a spectral width of 2000Hz, severely limiting the maximum echo train length (ETL). Higher field magnets (37) would not only provide increased signal, but greater spectral separation allowing shorter readouts and longer ETLs. However, there is an associated decrease in T_2 relaxation times at higher fields will further deteriorate later echoes (38).

In conclusion, studies of both physiological phantoms and healthy volunteers demonstrated the spectral sensitivity and spatial specificity of the new ME-COSI sequence.

Reproducibility studies using individual voxels extracted from ME-COSI data demonstrate reliability comparable to existing techniques like L-COSY. Further acceleration of the sequence and improved characterization of the effects of T_2 losses on multi-echo acquisition could help bring the sequence to clinical viability.

Acknowledgments

The authors would like to acknowledge the scientific support of Dr. Mark Brown and Dr, Yutaka Natsuaki of Siemens Medical Systems, USA, Dr. Jonathan Furuyama and Mr. Neil Wilson. The authors would also like to acknowledge the MRI technicians at 300 Medical Plaza MRI facility for their technical support.

This work was funded by an NIH grant (1R01MH089565) and two IDEA grants from the US Army Breast and Prostate Cancer Research Programs (BCRP# W81XWH-04-01-0565 and PCRP# #W81XWH-04-1-0885)

REFERENCES

1. Ernst, RR.; Bodenhausen, G.; Wokaun, A. Two-Dimensional NMR Spectroscopy. Oxford: Clarendon Press; 1987. Principles of Nuclear Magnetic Resonance in one and two dimensions; p. 610
2. Friebolin, H. Two-dimensional NMR Spectroscopy. 3rd Edition. New York: Wiley-VCH publications; 1998. Basic one- and two-dimensional NMR Spectroscopy; p. 231-285.
3. Thomas MA, Yue K, Binesh N, et al. Localized Two-dimensional Shift Correlated MR Spectroscopy of Human Brain. Magn Reson Med. 2001; 46:58–67. [PubMed: 11443711]
4. Binesh N, Yue K, Fairbanks L, Thomas MA. Reproducibility of localized 2D Correlated MR Spectroscopy. Magn Reson Med. 2002; 48:942–948. [PubMed: 12465102]
5. Thomas MA, Hattori N, Umeda M, Sawada T, Naruse S. Adding a new spectral dimension to localized 3T 1H MR Spectroscopy- From Phantoms to Human Brain in vivo. NMR Biomed. 2003; 16:245–251. [PubMed: 14648883]
6. Velan SS, Said N, Durst C, et al. Distinct patterns of fat metabolism in skeletal muscle of normal weight, overweight and obese humans. Am J Physiol Regul Integ Comp Physiol. 2008; 295:R1060–R1065.
7. Velan SS, Durst C, Lemieux SK, et al. Investigation of Muscle Lipid Metabolism by Localized One- and Two-Dimensional MRS Techniques using a Clinical 3T MRI/MRS Scanner. J. Magn Reson Imag. 2007; 25:192–199.
8. Brown TR, Kincaid BM, Ugurbil K. NMR Chemical shift imaging in three dimensions. Proc Natl Acad Sci USA. 1982; 79:3523. [PubMed: 6954498]
9. Hwang JH, Pan JW, Hetherington HP, Stein DT. Regional differences in intramyocellular lipids in humans observed by in vivo 1H MR spectroscopic imaging. J Appl Physiol. 2001; 90:1267–1274. [PubMed: 11247923]
10. Pohmann R, von Kienlin M, Haase A. Theoretical evaluation and comparison of fast chemical shift imaging methods. J Magn Reson. 1997; 129:145–160. [PubMed: 9441879]
11. Aue WP, Bartholdi E, Ernst RR. Two dimensional Spectroscopy. Application to nuclear magnetic resonance. J Chem Phys. 1976; 64:2229–2246.
12. Hennig J, Nauerth A, Friedburg H. RARE imaging: A fast imaging method for clinical MR. Magn Reson Med. 1986; 3:823–833. [PubMed: 3821461]
13. Constable R, Smith R, Gore J. Signal-to-Noise and Contrast in Fast Spin Echo (FSE) and Inversion Recovery FSE Imaging. J Comp Assist Tomogr. 1992; 16(1):41–47.
14. Listerud J, Einstein S, Outwater E, Kressel HY. First principles of fast spin echo. Magn Reson Q. 1992; 8(4):199–244. [PubMed: 1489675]
15. Duyn JH, Moonen CTW. Fast proton spectroscopic imaging of human brain using multiple spin-echoes. Magn Reson Med. 1993; 30:409–414. [PubMed: 8255188]
16. Dydak U, Meier D, Lamerichs R, Boesiger P. Trading Spectral Separation at 3T for Acquisition Speed in Multi Spin-Echo Spectroscopic Imaging. AJNR. 2006; 27:1441–1446. [PubMed: 16908554]

17. Rutgers DR, van der Grond J. Relaxation times of choline, creatine and N-acetyl aspartate in human cerebral white matter at 1.5T. NMR Biomed. 2002; 3:215–221. [PubMed: 11968137]
18. Mlyanarik V, Gruber S, Moser E. Proton T(1) and T(2) relaxation times of human brain metabolites at 3 Tesla. NMR Biomed. 2001; 5:325–331.
19. Feinberg D, Mills C, Posin J, et al. Multiple Spin-Echo Magnetic Resonance Imaging. Radiology. 1985; 155:437–442. [PubMed: 3983396]
20. Barker G, Mareci T. Suppression of Artifacts in Multiple-Echo Magnetic Resonance. J Magn Reson. 1988; 83:11–28.
21. Ogg R, Kingsley P, Taylor J. WET, a T1- and B1-insensitive water-suppression method for in vivo localized 1H NMR spectroscopy. J Magn Reson B. 1994; 104(1):1–10. [PubMed: 8025810]
22. Le Roux P, Gilles RJ, McKinnon GC, Carlier PG. Optimized outer volume suppression for single-shot fast spin-echo cardiac imaging. J Magn Reson Imaging. 1998; 8:1022–1032. [PubMed: 9786138]
23. Govindaraju V, Young K, Maudsley AA. Proton NMR chemical shifts and coupling constants for brain metabolites. NMR Biomed. 2000; 13(3):129–153. [PubMed: 10861994]
24. Brown M. Time-domain combination of MR spectroscopy data acquired using phased-array coils. Magn Reson Med. 2004; 52:1207–1213. [PubMed: 15508170]
25. Klose U. In vivo proton spectroscopy in presence of eddy currents. Magn Reson Med. 1990; 14:26–30. [PubMed: 2161984]
26. Soila KP, Viamonte M, Starewicz PM. Chemical shift misregistration effect in magnetic resonance imaging. Radiology. 1984; 153:819–820. [PubMed: 6494479]
27. Kreis R, Jung B, Slotboom J, Felblinger J, Boesch C. Effect of exercise on the creatine resonances in H-1 MR spectra of human skeletal muscle. J Magn Reson. 1999; 137:350–357. [PubMed: 10089169]
28. Velan SS, Lemieux R, Raylman W, Boling G. Detection of cerebral metabolites by single-voxel-based PRESS and COSY techniques at 3T. J Magn Reson Imag. 2007; 265:405–409.
29. Rémy C, Grand S, Laï ES, et al. 1H MRS of human brain abscesses in vivo and in vitro. Magn Reson Med. 2005; 34:508–514.
30. Cheng LL, Chang IW, Louis DN, Gonzalez RG. Correlation of High-Resolution Magic Angle Spinning Proton Magnetic Resonance Spectroscopy with Histopathology of Intact Human Brain Tumor Specimens. Cancer Research. 1998; 58:1825–1832. [PubMed: 9581820]
31. Kreis R, Boesch C. Spatially localized, one- and two-dimensional NMR spectroscopy and in vivo application to human muscle. J Magn Reson B. 1996; 113:103–118. [PubMed: 8948135]
32. Mulkern RV, Wong STS, Winalski C, Jolesz FA. Contrast manipulation and artifact assessment of 2D and 3D RARE sequences. J Magn Reson. 1990; 8:557–566.
33. Mlyanarik V, Gruber S, Moser E. Proton T(1) and T(2) relaxation times of human brain metabolites at 3 Tesla. NMR Biomed. 2001; 5:325–331.
34. Lipnick S, Verma G, Ramadan S, Furuyama J, Thomas MA. Echo planar correlated spectroscopic imaging: Implementation and pilot evaluation in human calf in vivo. Magn Reson Med. 2010; 64:947–956. [PubMed: 20574964]
35. Jezzard P, Barnett A. Pierpaoli. Characterization of and correction for eddy current artifacts in echo planar diffusion imaging. Magn Reson Med. 1998; 39:801–812. [PubMed: 9581612]
36. Dydak, U.; Weiger, M.; Pruessmann, K., et al. Scan Time Reduction in Spectroscopic Imaging using SENSE; Proceedings of the 7th Annual Meeting of ISMRM; Philadelphia: 1999. p. 679
37. Otazo R, Mueller B, Ugurbil K, et al. Signal-to-noise ratio and spectral linewidth improvements between 1.5 and 7 Tesla in proton echo-planar spectroscopic imaging. Magn Reson Med. 2006; 56:1200–1210. [PubMed: 17094090]
38. Michaeli S, Garwood M, Zhu X, et al. Proton T_2 relaxation study of water, N-acetylaspartate, and creatine in human brain using Hahn and Carr-Purcell spin echoes at 4T and 7T. Magn Reson Med. 2002; 47:629–633. [PubMed: 11948722]

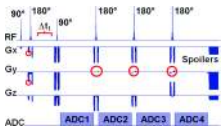

Figure 1.
The pulse diagram of the Multi-Echo Correlated Spectroscopic Imaging (ME-COSI) sequence. This sequence shows an echo train length (ETL) of four, with four phase encoding steps and readout events per TR. Phase-encoding gradients are circled in red. Note the diagram is not drawn to scale.

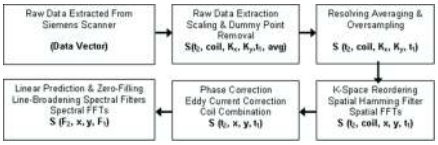

Figure 2.

A flow chart of post processing steps performed in reconstruction of 4D ME-COSI spectra from the raw file obtained from the 3T Siemens Tim-Trio scanner.

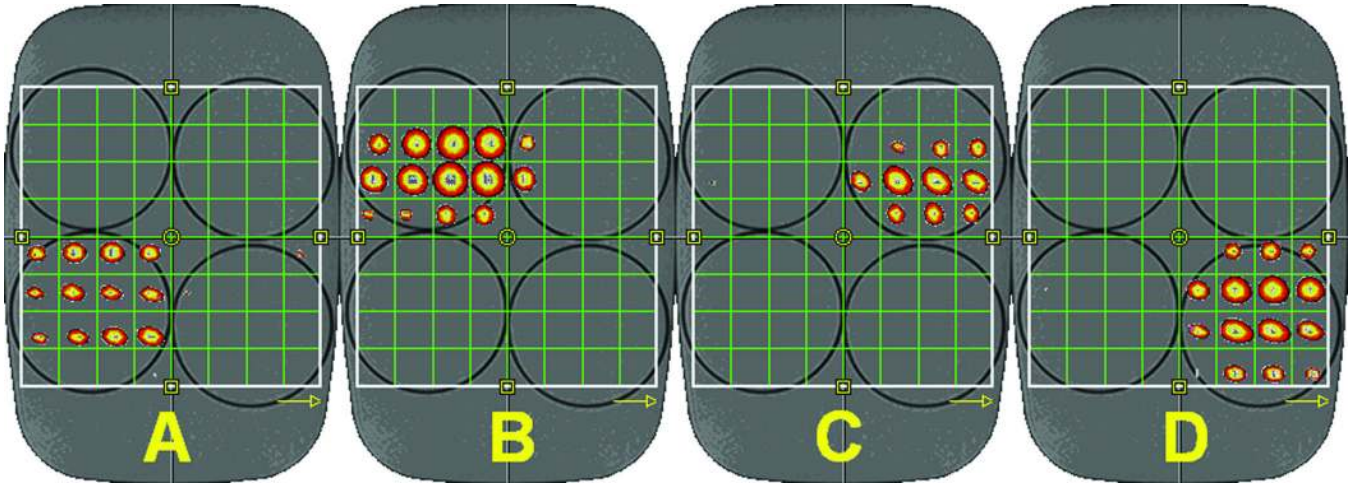

Figure 3.
ME-COSI spectra taken from an 8×8 array of 0.98 mL voxels in the quad phantom. Spatial profiles of the cross peaks from Lac (A) and the diagonal peaks from Ch (B), NAA (C) and Cr (D), are shown against the T_1-weighted MRI localization.

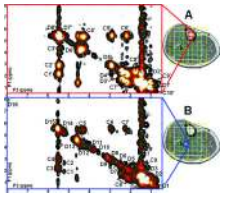

Figure 4.
ME-COSI spectra from the calf muscle of a 54 year-old volunteer. Tables 3 and 4 show peak assignment tables for metabolites detected in tibial marrow (top) and soleus muscle (bottom), respectively.

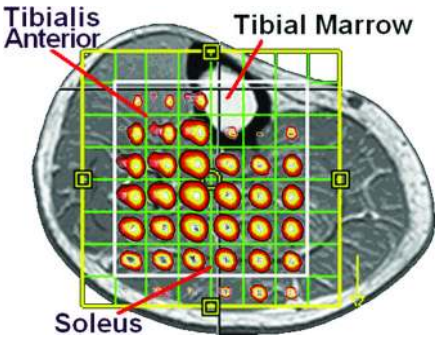

Figure 5.
ME-COSI spectra showing the spatial profile of the 3.9 ppm diagonal peak of Cr over an 8×8 array of 2.0 ml voxels in the calf. Peak-splitting is apparent in the area of the tibialis anterior muscle and no creatine is observed in the area of the tibial marrow.

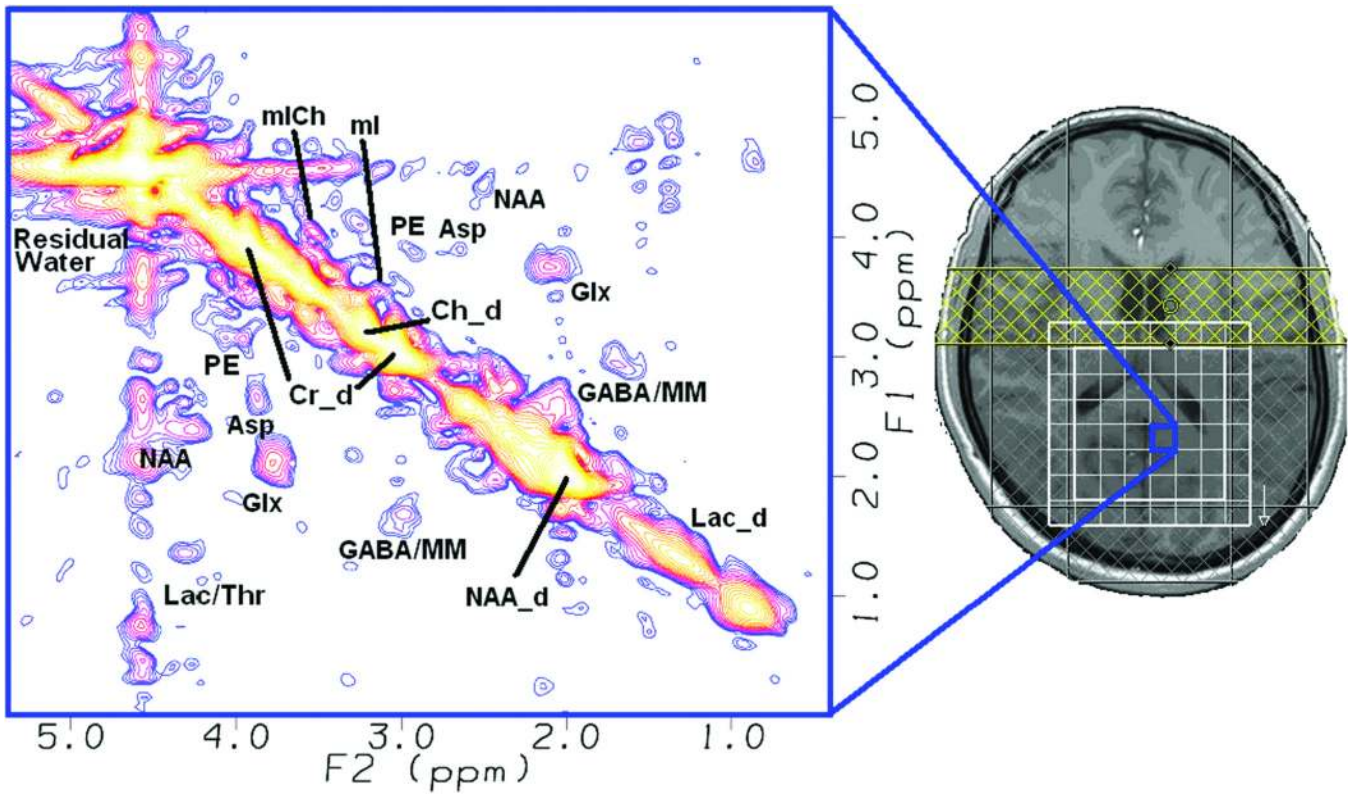

Figure 6.

An ME-COSI spectrum taken from a 4.0 ml voxel from the occipital lobe of a healthy 27 year-old volunteer. Diagonal peaks due to water, Ch_d, Cr_d, NAA_d and Lac_d are labeled, as are the cross-peak of NAA, PE, mI, mICh, Lac/Thr, Asp, Glx and GABA/MM.

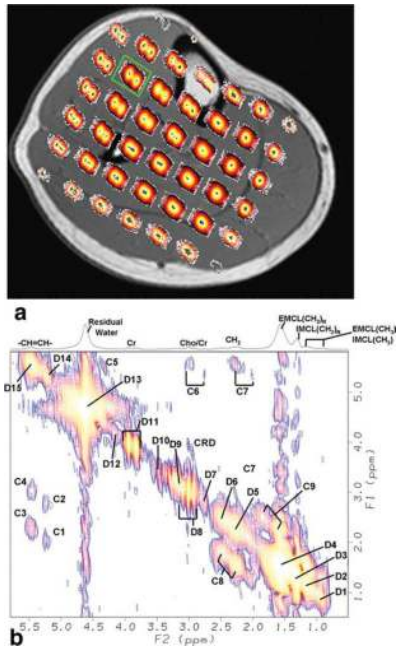

Figure 7.

ME-COSI spectra showing the spatial profiles of the 3.0 ppm diagonal peak of Cr (A), the [F1,F2] = 2.0, 3.6 ppm cross peak due to Glx (B) and the [F1,F2] = 3.0, 3.5 ppm cross peak due to mI (C). The 8×8 array of 4.0 ml voxels in the occipital lobe of a 24 year-old volunteer has been superimposed against the MRI localization.

Table 1

Assignment of 2D diagonal and cross peaks detected by ME-COSI in the tibial marrow.

Peak	Proton	F_2 (ppm)	F_1 (ppm)
D1'	CH_3-$(CH_2)_N$	0.9	0.9
D2'	-$(CH_2)_N$-	1.3	1.3
D3'	CH_2CH=CH	2.0	2.0
D4'	$CH_2OCOCH_2CH_2$	2.2	2.2
D5'	-CH=CHCH_2CH=CH-	2.9	2.9
D6'	ROCH-CH_2OCOR	4.2	4.2
D7'	ROCH-CH_2OCOR	5.3	5.3
D8'	-CH=CH-	5.3	5.3
C1'	CH_2CH=CH	5.4	2.2
C2'	-CH=CHCH_2CH=CH-	5.4	2.9
C3'	ROCH-CH_2OCOR	5.1	4.2
C4'	ROCH-CH_2OCOR	4.2	5.1
C5'	-CH=CHCH_2CH=CH-	2.9	5.3
C6'	CH_2CH=CH	2.2	5.3
C7'	$CH_2OCOCH_2CH_2$	2.1	1.4
C8'	$CH_2OCOCH_2CH_2$	1.4	2.0
C9'	-CH_2-CH_3	1.2	0.9
C10'	-CH_2-CH_3	0.9	1.2

Table 2

Assignment of 2D diagonal and cross peaks detected by ME-COSI in the soleus muscle.

Peak	Proton	F_2 (ppm)	F_1 (ppm)
D1	CH_3 (IMCL)	0.9	0.9
D2	CH_3 (EMCL)	1.0	1.0
D3	$(CH_2)_N$ (IMCL)	1.3	1.3
D4	$(CH_2)_N$ (EMCL)	1.4	1.4
D5	C**H**$_2$CH=CH	2.0	2.0
D6	$CH_2OCOCH_2CH_2$	2.2	2.2
D7	-CH=CHC**H**$_2$CH=CH-	2.7	2.7
D8	-CH=CHC**H**$_2$CH=CH & N-CH_3 (Cr)	3.0	3.0
D9	TMA (Ch)*	3.2	3.2
D10	Taurine (Tau)	3.4	3.4
D11	N-CH_2 (Cr)	3.9	3.9
D12	ROCH-C**H**$_2$OCOR ^	4.3	4.3
D13	H_2O (Water)	4.7	4.7
D14	-CH=CH-(IMCL) & ROC**H**-CH_2OCOR	5.4	5.4
D15	-CH=CH- (EMCL)	5.6	5.6
D16	Carnosine	8.0	8.0
C1	IMCL(-C**H**=C**H**-CH_2)	5.4	2.2
C2	IMCL (-C**H** =C**H**-CH_2)	5.4	2.9
C3	EMCL(-C**H** =C**H**-CH_2)	5.6	2.2
C4	EMCL(-C**H** =C**H**-CH_2)	5.6	2.9
C5	ROC**H**-C**H**$_2$OCOR	4.2	5.4
C6	EMCL/IMCL	5.6	2.9
C7	EMCL/IMCL	2.8	5.5
C8	C**H**$_2$-C**H**$_2$	2.5	1.5
C9	C**H**$_2$-C**H**$_2$	1.5	2.5

Table 3

Coefficients of variation of S/S_{Cr} for various metabolites measured across 32 scans of the brain phantom with the ME-COSI sequence. F_1 and F_2 peak locations are indicated for both diagonal and cross peaks. The CV of Cr was measured by comparing the 3.9 ppm peak of Cr to the 3.0 ppm peak used for reference.

Name	Metabolite	Type	F_1 (ppm)	F_2 (ppm)	CV (%)
Cr39	Creatine	Diag	3.9	3.9	**7.8**
mI	Myo-Inositol	Diag	3.5	3.5	**6.2**
Ch	Choline	Diag	3.2	3.2	**5.8**
NAA	N-Acetyl Aspartate	Diag	2.0	2.0	**5.1**
Lac	Lactate	Diag	1.3	1.3	**11.8**
mI	Myo-Inositol	Cross	3.5	3.1	**7.0**
Glx	Glutamine/Glutmate	Cross	3.6	2.0	**5.3**
Asp	Aspartate	Cross	3.8	2.8	**8.2**
PE	Phosphoethanolamine	Cross	3.9	3.2	**10.5**
mICh	Myo-Inositol Choline	Cross	4.0	3.5	**11.0**
NAA	N-Acetyl Aspartate	Cross	4.3	2.6	**7.8**
GABA/MM	γ-aminobutyric Acid & macromolecules	Cross	3.0	1.8	**12.1**
GSH	Glutathione	Cross	4.5	2.9	**17.3**
Lac	Lactate	Cross	4.1	1.3	**24.7**

Table 4

Coefficients of Variation of S/S_{Cr} for various metabolite peaks recorded in five intra-subject and eight inter-subject brain studies with the ME-COSI sequence.

Name	Metabolite	Type	F_1 (ppm)	F_2 (ppm)	Intra CV (%)	Inter CV (%)
Cr39	Creatine	Diag	3.9	3.9	**7.1**	**7.6**
mI	Myo-Inositol	Diag	3.5	3.5	**7.4**	**7.9**
Ch	Choline	Diag	3.2	3.2	**3.6**	**6.0**
NAA	N-Acetyl Aspartate	Diag	2.0	2.0	**3.5**	**9.1**
NAA	N-Acetyl Aspartate	Cross	4.3	2.6	**16.8**	**16.8**
Glx	Glutamine/Glutamate	Cross	3.6	2.0	**9.5**	**13.1**
PE	Phosphoethanolamine	Cross	3.9	3.2	**14.6**	**14.0**
Asp	Aspartate	Cross	3.8	2.8	**8.7**	**17.5**
GABA/MM	γ-aminobutyric Acid & macromolecules	Cross	3.0	1.8	**8.9**	**12.0**
Lac	Lactate	Cross	4.1	1.3	**9.9**	**14.0**